



Agglomeration of the bed material in fluidized bed reactors for thermal conversion of biomass - A threat for the development of the technology

Britt-Marie Steenari^{*}, Lars-Erik Åmand^{**} and Jessica Bohwalli^{**}

^{*}Chalmers University of Technology, Department of Chemical and Biological Engineering, division of Environmental Inorganic Chemistry and Industrial Materials Recycling, SE-412 96 Göteborg, Sweden

^{**}Chalmers University of Technology, Department of Energy & Environment, division of Energy Technology, SE-412 96 Göteborg, Sweden

* corresponding author

ABSTRACT

Thermal conversion of biomass in fluidized bed systems for the production of heat and power and in the future also transportation fuels for vehicles through a gasification process need supply of biomass from various sources. These biomass fuels can vary a lot in quality and quantity. Many biomass types and waste derived fuels contain salts of alkali metals, i.e. potassium and sodium salts. When these alkali metals are released during combustion in fluidized bed systems using a bed material such as silica sand, agglomeration of the bed material may occur during unfavorable conditions. Thus, a significant amount of work has been put into the investigations of sintering mechanisms and the development of methods to prevent bed material sintering. In the present work combustion of alkali metal rich fuels alone and in combinations has been studied in the 12 MW_{th} circulating fluidized bed (CFB) boiler located at the campus area of Chalmers University of Technology.

Keywords: *CFB, biomass combustion, refuse derived fuel, material sintering, agglomeration, ash fouling*

1. INTRODUCTION

Combustion of biomass, such as forestry residues and straw, is often hampered by ash sintering, fouling and corrosion. Similar problems are encountered when firing municipal solid waste and other waste derived fuels that consist of a mixture of paper, wood, plastics and textiles. These problems are all caused by the alkali metal compounds present in the fuel ash part or formed during combustion. These compounds have low melting temperatures and high vapour pressure even at moderate temperatures, such as around 700°C. For a fluidised bed boiler unit with its silica based bed sand ash, the presence of alkali metal compounds is especially detrimental since silica forms eutectic melts at combustion temperatures with both sodium and potassium species. Sintering of the bed material due to formation of sticky surface layers on the sand particles can, in the worst case, lead to defluidization and total bed solification.

Condensation of vapourized alkali metal salts have been shown to start the fouling of super heater tubes and to contribute dramatically to corrosion processes in the super heater area [1-2]. Due to these problems, all related to biomass and waste combustion, an

extensive amount of work has been put into investigations of the mechanisms involved and of various methods to abate the problems. Co-combustion of troublesome fuels with fuels containing aluminium silicates, iron compounds and sulphur such as municipal sewage sludge have been used to create a better total ash composition and to transfer alkali metal chlorides to the less corrosive sulphates [7]. In addition, the use of additives, such as kaolin and ammonium sulphate, has been studied, also with the aim to transfer alkali metal salts to less problematic compounds [5-6].

In the present work we focused on the close investigation of the ash layers formed on bed material particles from a circulating fluidised bed boiler during three combustion tests: Case Wood-Straw; Case Bark and Case RDF. The aim was to elucidate the mechanisms of the on-set of formation of sticky layers on the sand particles, a process that can lead to total bed de-fluidisation in the worst case and shut down of the boiler.

2. Materials and methods

2.1 Research boiler and operating conditions

The work presented in this paper was part of a large research program including combustion issues, ash sintering and alkali metal chemistry as well as investigations of super heater corrosion [5-7]. Figure 1 shows a schematic sketch of the 12 MW circulating fluidised bed (CFB) boiler located at Chalmers University of Technology.

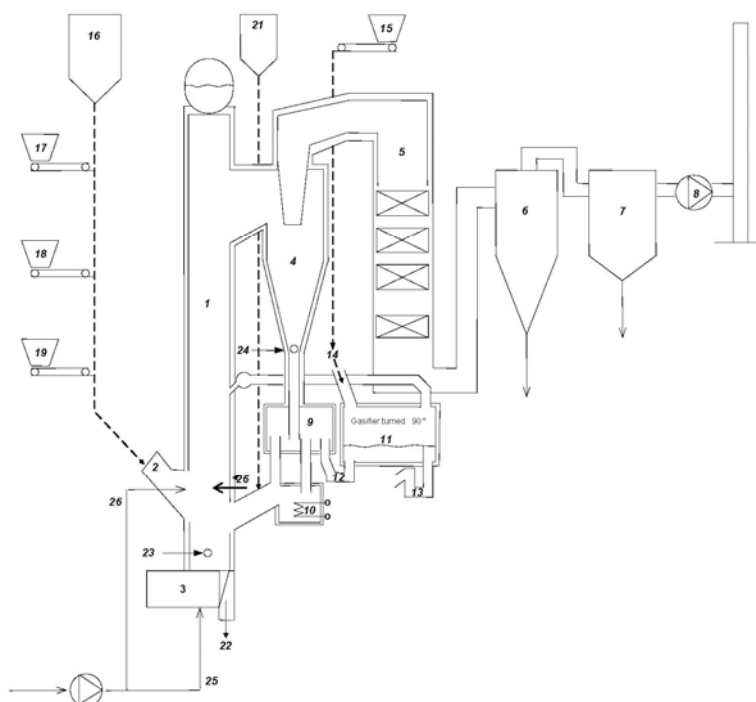


Figure 1. Overview of the Chalmers CFB research boiler facility with the gasifier included. 1: furnace, 2: fuel feeding to furnace, 3: wind box, 4: cyclone, 5: convection pass, 6: secondary cyclone, 7: bag house filter, 8: flue gas fan, 9: particle distributor, 10: particle cooler, 11: gasifier, 12: particle seal 1, 13: particle seal 2, 14: fuel feeding (gasifier), 15: fuel hopper (gasifier), 16: hopper for bed material (quartz sand), 17: fuel hopper 1, 18: fuel hopper 2, 19: fuel hopper 3, 22: ash removal, 23: position for bed sample. 24: position for cyclone leg, 25: primary air flow, 26: secondary air flow.



The combustion chamber (1) has a cross section of 2.25 m² and a height of 13.6 m. The various fuels are fed to the bottom of the bed through a fuel chute (2). The circulating material is separated at a primary cyclone (4) and returned to the combustion chamber through the cyclone leg (24) and particle distributor (9). An external heat exchanger (10) cools the circulating material before re-entering the combustion chamber when required. Primary air is introduced through air nozzles located at the bottom of the riser and secondary air 2.2 m above the bottom plate (26). The exhaust gas is cooled to 150 C in the convection pass (5). Effective soot blowers (using steam blown probes) are installed along each section of the convection pass. These soot blowers are used regularly to keep the flue gas temperature below 180 C (once or twice every 24 h). Fly ashes are separated in the secondary cyclone (6) and the textile filter (7). Silica sand ($d_p = 0.3$ mm) was used as bed material in all tests. The operating conditions are typical for a commercially operated CFB boiler. This means a fluidizing velocity of approx. 5 m/s in the top of the riser that leads to a proper circulation of bed material through the primary cyclone, good heat transfer of moving bed particles and an attrition of the fuel ash into fly ash, which is important in order to avoid accumulation of bottom bed ash. Typical operating conditions are also proper excess air ratio (20-25% excess air) and a bottom bed temperatures of 850C

Three combustion cases were included in this work:

Case Wood-Straw: Wheat straw (20 % on dry mass) was co-fired with a “clean” biomass consisting of saw dust from a saw mill pressed into wood pellets.

Case Bark: Forest residues consisting of 100 % bark crushed, dried and pressed into pellets.

Case RDF: Bark pellets were co-fired with a waste (refuse derived fuel) pellets produced by IcoPower in the Netherlands.

In addition, samples of agglomerated/sintered bed material (23, Figure 1) and agglomerated/sintered ash deposits found in the particle distributor (9 Figure 1) were analysed with the aim to show the reasons for agglomeration/sintering and fouling during biomass combustion and gasification in fluidized bed systems.

The element compositions of the fuels are given in Table 1.

2.2 Analytical methods

The main element concentrations in bed materials and ash samples were determined by an ICP-OES analyser (Inductive Coupled Plasma equipped with an Optical Emission Spectroscopy detector) after total dissolution. The samples are denoted BB for bottom bed ash and CB for return leg ash (24, Figure 1), whereas the samples of sintered ash are identified by the part of the boiler where it was found and the combustion case preceding the finding of the sintered material. The return leg position represents bed particles circulating in the hot loop of the CFB-boiler, a position normally suffering from severe agglomeration and plugging when using biomass rich in alkali.



Table 1. Fuel compositions

	Wood	Straw	Bark	RDF
Moisture %	8.5	9.5	10	5-15
Ash % dry	0.6	5.3	4.2	15
Element concentrations (% on dry fuel)				
C	50.5	49.5	52	46
H	6.0	6.1	5.8	6.2
O	43.4	43.8	37	32
S	0.01	0.08	0.03	0.2
N	0.06	0.46	0.48	0.77
Cl	0.02	0.27	0.02	0.53
Ash elements g/ kg dry ash				
K	138	157	46	11
Na	7.5	6.3	10	22
Al	6.7	4.0	26	48
Si	116	230	110	138
Fe	8.8	3.4	12	18
Ca	152	72.4	198	192
Mg	29.8	12.2	17	11
P	13	12	10	5.1
Ti	0.4	0.3	1	11
Ba	2.2	0.7	2.9	1.8
Effective heating value (H) MJ/kg				
H, dry basis	19.1	18.4	19.5	17.9
H, raw	17.1	15.5	18.6	17.7

The presence of ash layers on the bed material particles in sample material and the distribution of elements within sintered samples were studied using scanning electron microscopy coupled with energy dispersive X-ray fluorescence measurements (SEM-EDX). Specimens were prepared for SEM-EDX by embedding bed material particles in epoxy resin and grinding the specimen surface to expose cross-sections of a sufficient amount of representative particles. Silicon carbide grinding paper was used and the specimen surface was cleaned by ethanol after grinding to remove any loose particles.

The electron microscope used is a FEI Quanta 200 Field Emission Gun ESEM equipped with an INCA EDX detector and evaluation program. Since the present sample materials are not conducting the low vacuum mode was used to prevent sample surface charging. SEM micrographs were taken with a Solid State Detector in the back scattered electron mode. The image created by back scattered electrons does not give any topographic information, but it shows differences in specimen material density as differences in color in a grey scale. A heavier or denser sample material gets a lighter color than sample parts that are less dense or contain lighter elements.

The quantification of elements by the EDX detector has a detection limit of 1 % by weight.



3. RESULTS AND DISCUSSION

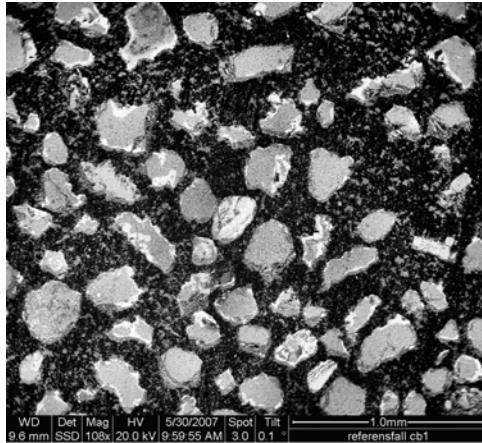
Table 2 shows the element composition of the ash samples included in this work. The most prominent difference between the samples is the Ca content, from 3% in the samples from combustion of *Wood-Straw* mixture to almost 13% in the *Bark* case. The sum content of K and Na is 3-4 % in all samples but potassium is generally the dominating alkali metal.

The element concentrations in a bulk sample of the sintered material are not very different from those of the bulk “*BB*” and “*CB*” samples. The composition is closest to the ash compositions from the *Wood-Straw* case with slightly higher contents of K and Ca.

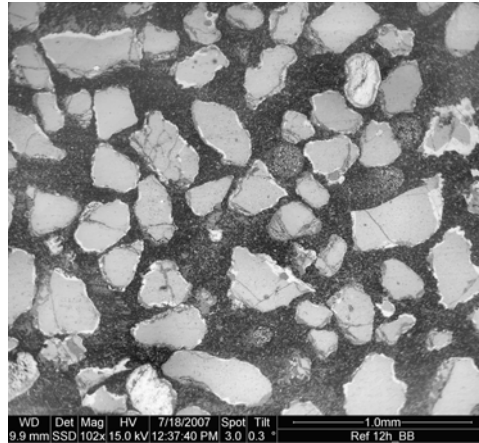
Table 2. Element concentrations (weight %) in ash samples. Denotations: BB=Bottom Bed, CB=Return leg

Test case/ Element	Wood-Straw		Bark		RDF		Sintered material in the return leg
	BB (12h)	CB (12h)	BB	CB	BB	CB	
Cl	<0.01	<0.01	0.01	0.01	<0.01	<0.01	<0.01
S	0.1	0.13	0.40	0.53	0.15	0.42	0.19
Al	0.85	0.62	1.55	2.62	1.19	1.77	0.83
Si	43.2	43.5	34.1	29.8	37.3	33.8	41.7
Fe	0.58	0.66	0.66	1.03	0.52	0.77	0.27
Ti	0.08	0.08	0.16	0.28	0.10	0.1	0.17
Mn	0.25	0.28	0.37	0.44	0.46	0.46	0.13
Mg	1.27	1.44	0.64	0.84	0.72	0.78	0.49
Ca	3.28	3.48	12.3	12.8	8.04	8.21	4.19
Ba	0.04	0.04	0.16	0.19	0.13	0.14	0.05
Na	0.34	0.28	0.80	0.89	0.57	0.57	0.45
K	2.56	2.10	2.00	2.24	3.28	3.68	3.28
P	0.20	0.18	0.36	0.49	0.42	0.54	0.20

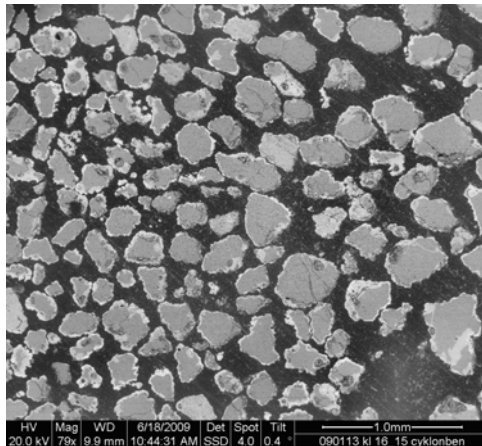
The use of back scattered electrons in producing images of sample particle cross sections gives the opportunity to easily get an overview of density differences. The ash layers on the sand particles are generally sintered and denser than the quartz sand which makes them clearly visible as a light area. Figure 2 shows overview pictures of samples *Wood-Straw*, *Bark* and *RDF*. In all samples ash layers on the sand particles are frequently occurring.



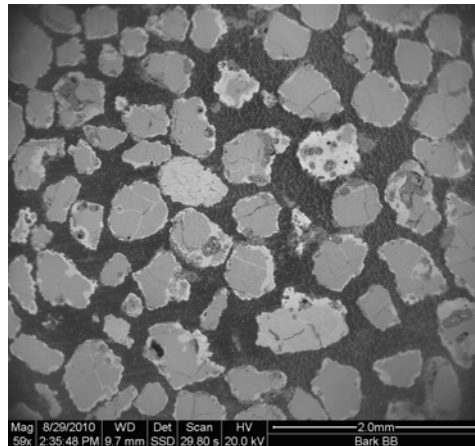
a) Wood-Straw “CB”



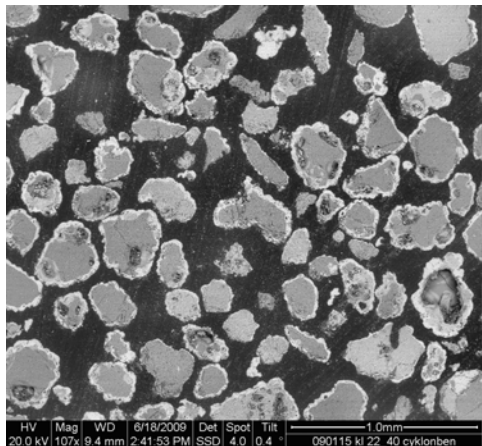
b) Wood-Straw “BB”



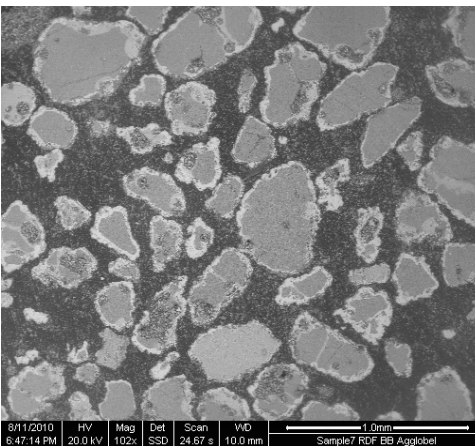
c) Bark “CB”



d) Bark “BB” (please observe the length scale)



e) RDF “CB”



f) RDF “BB”

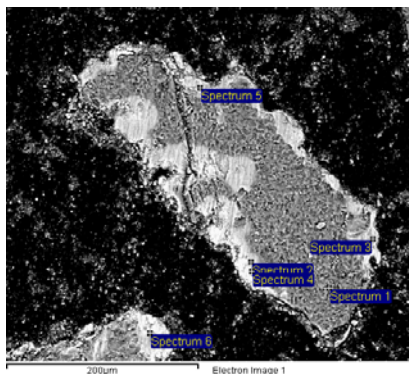
Figure 2. Back scattered electron images of bed sand particle cross sections for the three operating cases: *Wood-Straw*, *Bark* and *RDF* for samples taken either in the return leg position, “CB” (left) or bottom bed “BB” (right).

A closer look at the bed particles shows that the ash layers are not homogenous, but layers with different appearance and different composition can be seen. Figures 3-5 show

images with higher magnification and are examples from the cases *Wood-Straw*, *Bark* and *RDF*.

In Figure 3 Spectrum 1 represents the quartz composition, Spectrums 2, 5 and 6 originates in the alkali metal rich layer closest to the quartz surface, whereas Spectrums 3 and 4 show the composition of the outer calcium rich ash layer. The surface layer not only contains K and Ca oxides, but also Si. Obviously, potassium has been involved in the initial reaction since it is enriched in the inner layer. Calcium compounds have probably been incorporated in the layer later in the process due to entrapment of ash particles by the sticky potassium silicate phase.

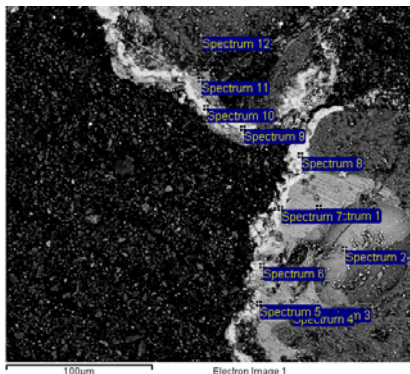
The surface layer structure is denser than that of the quartz and looks sintered and non-porous. The layer is not separate from the quartz particle but seems to have grown on the particle surface. EDX data for sand particles from the “*BB*” sample gave similar results.



Spectrum	O	Na	Mg	Si	P	K	Ca	Total
Spectrum 1 Quartz	47	0	0	51	0	0	1	100
Spectrum 2 Inner layer	49	1	1	32	0	8	8	100
Spectrum 5 Inner layer	52	1	1	36	0	6	3	100
Spectrum 6 Inner layer	51	1	2	33	0	8	5	100
Spectrum 3 Outer layer	54	0	6	20	2	1	15	100
Spectrum 4 Outer layer	47	0	6	19	2	1	23	100

Figure 3. Particle with ash layers on the surface, case *Wood-Straw* “*CB*”. Element concentrations (weight %) in marked points are shown in the table to the right.

The bed material (“*CB*”) particles from the case *Bark* shown in Figure 4 also show one inner layer containing 5-8 % K and 3-6% Ca along with significant amounts of Si. Occasionally, this layer also contains Na, but the dominating composition points at a mixture of potassium silicate and calcium silicate formed by reactions between potassium salts (KCl), calcium oxide (CaO) and silica (SiO₂). There is also an outer layer which appears as a structure with lighter color in the SEM picture. This layer is rich in Ca and has lower concentration of K than the inner layer has. The addition of Ca to this Si-K-Ca-O system leads to a higher melting point.



Spectrum		O	Na	Mg	Si	P	K	Ca	Total
Spectrum 3	Quartz	56	0	0	42	0	1	2	100
Spectrum 12	-"	58	0	0	40	0	1	2	100
Spectrum 1	Inner layer	55	13	1	34	0	5	3	100
Spectrum 2	-"	55	2	0	34	0	6	4	100
Spectrum 4	-"	50	1	1	35	0	7	6	100
Spectrum 11	-"	50	2	1	33	0	8	6	100
Spectrum 5	Outer layer	48	1	1	32	0	8	10	100
Spectrum 6	-"	50	1	2	27	0	5	11	100
Spectrum 7	-"	46	1	0	20	0	3	29	100
Spectrum 8	-"	46	0	0	21	0	1	31	100
Spectrum 9	-"	50	0	1	20	1	1	26	100
Spectrum 10	-"	47	0	3	21	0	2	27	100

Figure 4. Particle with ash layers on the surface, case *Bark* “*CB*”. Element concentrations (weight %) in marked points are shown in the table to the right.

When refuse derived fuel (RDF) was co-fired with bark in the case *RDF* more of Na appear in combination with K in the ash layers as shown in Figure 5 and the accompanying table. As in the case with bark as fuel the outer layer is high in Ca and this seems to lead to a stop in the growth of the ash layer in a similar manner as for the cases *Wood-Straw* and *Bark*.

No evidence of phosphorous being involved in the formation of ash layers on bed material particles was found in any of the combustion cases studied.

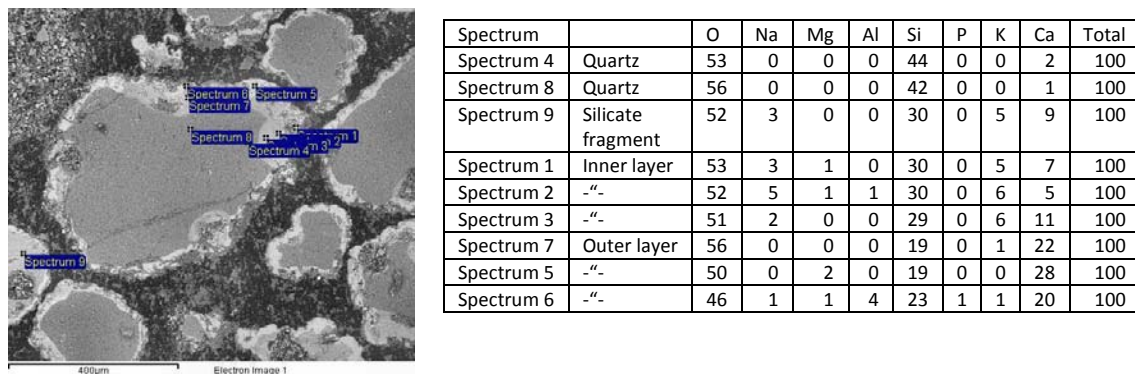


Figure 5. Particle with ash layers on the surface, case *RDF* “*BB*”. Element concentrations (weight %) in marked points are shown in the table to the right.

The data shown above indicate K/Ca ratios of about 1 in the inner layers on the bed material particles, whereas this ratio is much higher in the outer layers, going from about 10 in the *Bark* case to about 20 in the cases *Wood-Straw* and *RDF*. The ratios were calculated on a weight basis but as the molar weights of K and Ca are similar (39.1 g/mole and 40.1 g/mole respectively) they can be translated to molar ratios as well.

In order to investigate in more detail how the concentrations of important elements vary over the ash layers on the sand particles line scans were made, i.e. a number of point analyses were made along a line with the EDX detector.

Figure 6 and the accompanying diagrams shows a representative result for the sample *Bark* “*BB*”. The points are numbered 1-10 from the outer parts of the ash layer towards the inner quartz parts of the particle. It is clear that the concentration of K is highest in a layer closest to the quartz. This layer has a light grey color in the pictures and a dense, non-porous structure. Potassium concentrations as high as 15% were found in this layer, which means an important enrichment compared to the average composition (Table 2) with 2% K. The average Ca concentration in the *Bark* “*BB*” sample is 12% which can be compared to the concentration of about 20% in the outer surface layer. The concentration of K in that layer is similar to the average sample concentration. For some reason calcium compounds are enriched on the alkali silicate phase covering the sand particles and this results in solidification of the layer due to increase of the melting point of the mixture [3].

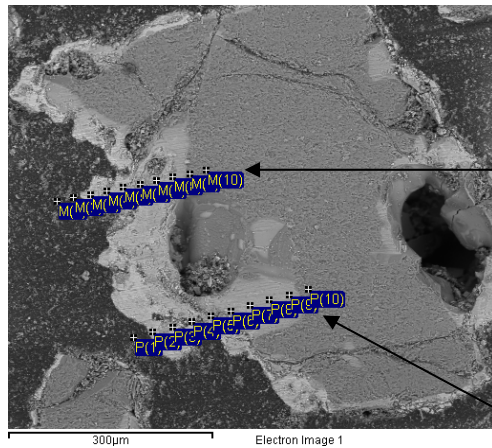
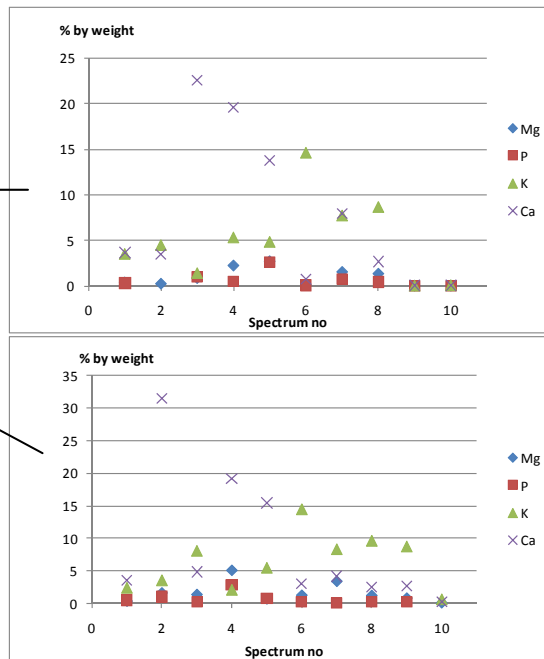


Figure 6. Two line scans, i.e. series of point analyses, over the ash layer on a sand particle from *Bark* “*BB*”. The diagrams to the right show element concentration in % by weight on the Y-axis and point number on the X-axis.



A similar line scan over a surface ash layer on a bed material (“*BB*”) particle from the case *RDF* is shown in Figure 7 and corresponding diagram. Here a significant amount of Na was found along with K in the most alkali metal rich part of the ash layer (6% K and 3% Na). A very clear difference between this alkali rich layer and the outer layer can be seen in this figure and diagram. The outermost layer is rich in Ca, relatively low in Si and contains small amounts of S and P as shown in Table 3.

Compared to the average composition of bed material collected in the Bottom bed in case *RDF*, (see Table 2) with 8% Ca, 3.5% K, 0.6% Na and about 35% Si, the composition of the inner ash layer is significantly enriched in K and Na, whereas the outer layer is four to five times enriched in Ca.

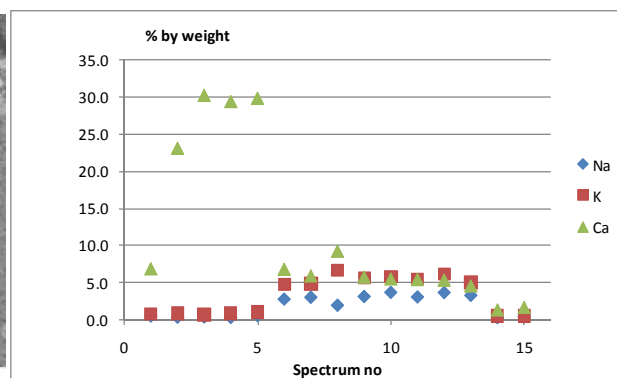
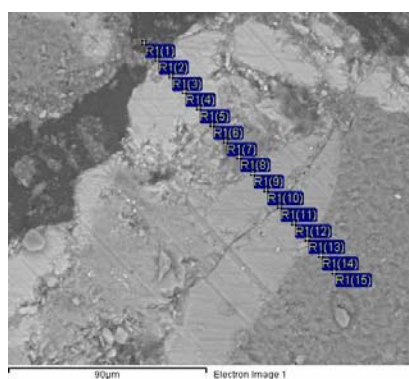


Figure 7. One series of point analyses, over the ash layer on a sand particle from *RDF* “*BB*”. The diagrams show element concentration in % by weight on the Y-axis and point number on the X-axis.

Table 3. Element concentrations (weight %) in the points shown in Figure 7.

Spectrum	R1(1)	R1(2)	R1(3)	R1(4)	R1(5)	R1(6)	R1(7)	R1(8)	R1(9)	R1(10)	R1(11)	R1(12)	R1(13)	R1(14)	R1(15)
O	55	48	49	49	49	52	53	44	53	51	52	51	53	59	56
Na	1	0	0	0	1	3	3	2	3	4	3	4	3	0	0
Si	35	14	17	18	18	32	32	36	32	33	33	33	34	38	41
P	0	2	1	0	0	0	0	0	0	0	0	0	0	0	0
S	0	3	1	0	0	0	0	1	0	0	0	0	0	0	0
K	1	1	1	1	1	5	5	7	6	6	6	6	5	1	1
Ca	7	23	30	29	30	7	6	9	6	5	5	5	5	1	2
Total	100	100	100	100	100	100	100	100	100	100	100	100	100	100	100

Only a few SEM images with corresponding EDX analysis data are shown here but they were chosen as representative examples out of a larger amount of data.

Samples of the agglomerated/sintered material found in the particle distributor (Figures 8 and 9) were subjected to the same type of investigations as the “BB” and “CB” samples described above with the aim to find possible mechanisms involved in the onset of agglomeration.



Figure 8. Agglomerated/sintered material found in the particle distributor, 9 in Figure 1.

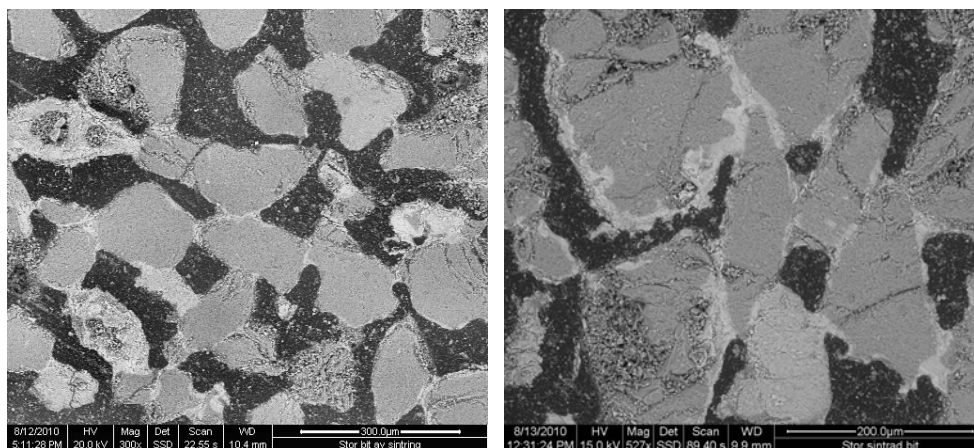


Figure 9. Cross section of the agglomerated/sintered material (SEM back scattered electron image)

EDX data show that the concentration of K in the bridging melt phase was 3-15% and the Ca concentration 2-10% with most points lying in the lower range.

Closer analysis of several parts of the bridging melt phase confirmed a relatively high concentration of K combined with a low concentration of Ca. A typical result is shown in Figure 10.

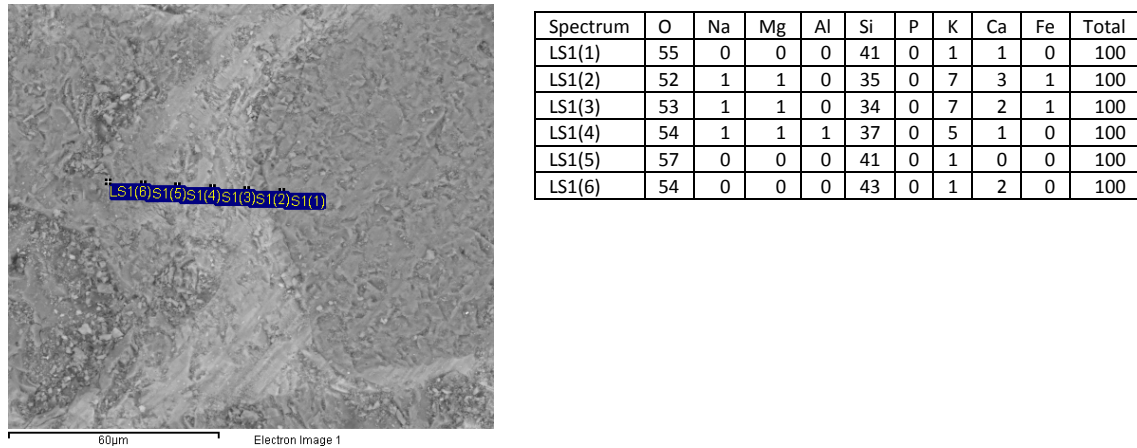


Figure 10. Bridging melt phase connecting sand particles in agglomerated/sintered material to the left. Corresponding element concentrations in weight % from the EDX are given in the table to the right.

EDX mapping results obtained for the sintered material show that the binding melt phase is in fact a potassium silicate melt (Figure 11). An interesting detail that could be seen here is that calcium occurs in spots and more or less separate from potassium in the bridging phase between sand particles. This is not similar to what was found for the non-sintered bed material samples where Ca was found to be present in an exterior, continuous phase covering the sand particles and their potassium silicate surface layer. The occurrence of Ca in crystals and not in a continuous phase was verified by further SEM investigations. That data also verified that the Ca-rich crystals were surrounded by K-rich silicate melt.

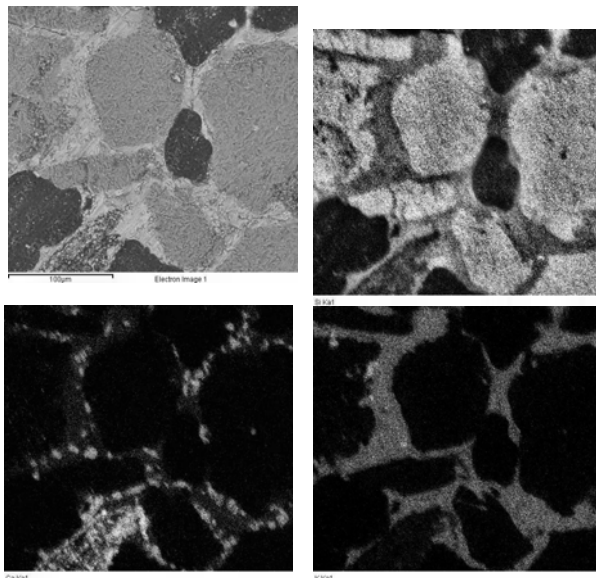


Figure 11. EDX mapping results for the sintered ash from the particle distributor.

 Upper left: Back scattered electron image

 Upper right: Si map

 Lower left: Ca map

 Lower right K map

Sintered lumps, mainly consisting of straw ash have been found in bed material samples when co-combustion of straw and wood has been applied [5]. Figure 12 shows such a sample with a straw ash “stone” marked out. Figure 13 shows EDX mapping results obtained for a rather big straw ash stone. Similar to what was found for the bridging melt phase in the sintered material from the return leg, this straw ash stone is held together by a potassium silicate melt low in calcium. An ash composition high in potassium and silica while rather low in calcium is typical of straw [4]. We therefore conclude that it is probable that the onset of sintering in the return leg was caused by sticky fragments of straw ash rich in potassium silicate being deposited in this region. The amount of calcium rich ash from the wood fuel (bark) in these particles is not high enough to hinder further sintering as was the case for ash layers formed on quartz particles in the bed.

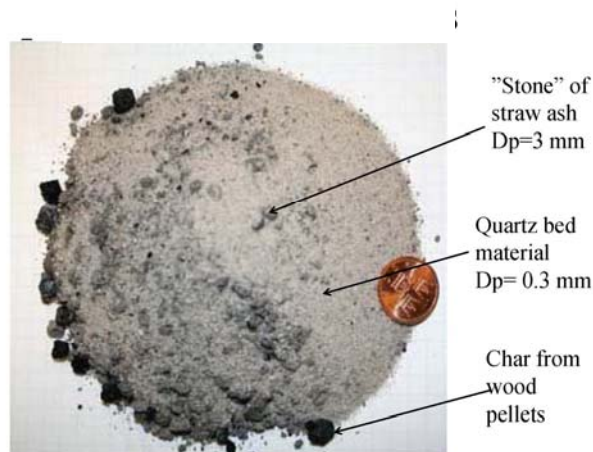


Figure 12. Photograph of bed material from co-combustion of wood and straw with “stones” of sintered straw ash.

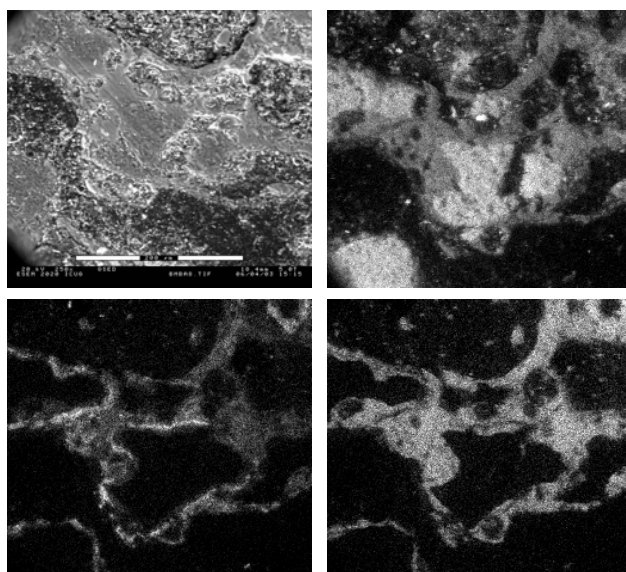


Figure 13. EDX mapping results for the sintered ash from the return leg.
Upper left: Back scattered electron image
Upper right: Si map
Lower left: Ca map
Lower right: K map



CONCLUSIONS

Three combustion cases with biomass and refuse derived fuel combinations were studied in this work. Wheat straw (20 % on dry mass) was co-fired with a “clean” biomass consisting of saw dust from a saw mill pressed into wood pellets. This case was compared to combustion of forest residues consisting of bark crushed, dried and pressed into pellets. The bark pellets case was compared to the straw case as well as to a case where the bark was co-fired with waste (refuse derived fuel) pellets produced by IcoPower in the Netherlands. In all three cases alkali metals form layers of alkali silicates on the quartz bed particles. A dual layer on the bed particles was identified with an inner layer rich in potassium and an outer layer rich in calcium. When the RDF was included in the fuel mix also sodium was present in the inner ash layer together with potassium and silica.

The growth of the ash layers seems to be stopped by the inclusion of calcium compounds giving a mixture with higher melting temperature enclosing the sticky alkali metal silicate layer. It is probable that the onset of sintering in the return leg was caused by sticky fragments of straw ash rich in potassium silicate being deposited in this region. The amount of calcium rich ash from the fuel (bark) in these particles is not high enough to hinder further sintering as was the case for ash layers formed on quartz particles in the bed.

The results did not show any sign of phosphorous being involved in the formation of ash eutectics on the bed particle surfaces.

4. REFERENCES

- [1] J. Pettersson, H. Asteman, J-E. Svensson, L-G. Johansson, KCl Induced Corrosion of a 304-type Austenitic Stainless Steel at 600°C; The Role of Potassium, Oxidation of Metals, 64(1 - 2) (2005) 23-41
- [2] C. Pettersson, L-G. Johansson, J-E. Svensson, The Influence of Small Amounts of KCl(s) on the Initial Stages of the Corrosion of Alloy Sanicro 28 at 600°C, Oxidation of Metals, 70(5-6) (2008) 241-256
- [3] M. Öhman, A. Nordin, B-J. Skrifvars, R. Backman, M. Hupa, Bed Agglomeration Characteristics during Fluidized Bed Combustion of Biomass Fuels, Energy & Fuels, 14 (2000) 169-178
- [4] B-M. Steenari, O. Lindqvist, High Temperature Reactions of Straw Ash and the Anti-sintering Additives Kaolin and Dolomite, Biomass and Bioenergy, 14(1998)67-76
- [5] K. Davidsson, D. Eskilsson, M. Gyllenhammar, S. Herstad Svärd, H. Kassman, B-M. Steenari, L-E. Åmand, Measures for simultaneous minimization of alkali related operating problems, Phase 1, Värmeforsk Report 997, 2006.



[6] M. Gyllenhammar, S. Herstad Svärd, K. Davidsson, L-E. Åmand, B-M. Steenari, N. Folkesson, J. Pettersson, J-E. Svensson, A. Boss, L. Johansson, H. Kassman, Measures for simultaneous minimization of alkali related operating problems, Phase 2, Värmeforsk Report 1037, 2007.

[7] S. Herstad Svärd, B-M. Steenari, L-E. Åmand, J. Bowalli, J. Öhlin, J. Pettersson, S. Karlsson, E. Larsson, J-E. Svensson, L-G. Johansson, K. Davidsson, L. Bäfver, M. Almark, Measures for simultaneous minimization of alkali related operating problems, Phase 3, Värmeforsk Report Project A08-817, 2010.

5. ACKNOWLEDGEMENTS

This project was financed by Värmeforsk AB (project: A08-817) and by the Swedish Energy Administration. The practical support from the operator at Akademiska Hus AB and the research engineers employed by Chalmers University of Technology is also greatly appreciated.